

Effect of Zn doping on the antiferromagnetism in kagome $\text{Cu}_{4-x}\text{Zn}_x(\text{OH})_6\text{FBr}$

Zili Feng,^{1,2} Yuan Wei,^{1,2} Ran Liu,¹ Dayu Yan,^{1,2} Yan-Cheng Wang,^{1,3} Jianlin Luo,^{1,2,4} Anatoliy Senyshyn,⁵ Clarina dela Cruz,⁶ Wei Yi,⁷ Jia-Wei Mei,⁸ Zi Yang Meng,^{1,9} Youguo Shi,^{1,*} and Shiliang Li^{1,2,4,†}

¹*Beijing National Laboratory for Condensed Matter Physics,
Institute of Physics, Chinese Academy of Sciences, Beijing 100190, China*

²*School of Physical Sciences, University of Chinese Academy of Sciences, Beijing 100190, China*

³*School of Physical Science and Technology, China University of Mining and Technology, Xuzhou 221116, China*

⁴*Collaborative Innovation Center of Quantum Matter, Beijing 100190, China*

⁵*Heinz Maier-Leibnitz Zentrum (MLZ), Technische Universität München, Garching D-85747, Germany*

⁶*Quantum Condensed Matter Division, Oak Ridge National Laboratory, Oak Ridge, Tennessee 37831, USA*

⁷*Semiconductor Device Materials Group, National Institute for
Materials Science, 1-1 Namiki, Tsukuba, Ibaraki 305-0044, Japan*

⁸*Institute for Quantum Science and Engineering, and Department of Physics,
Southern University of Science and Technology, Shenzhen 518055, China*

⁹*CAS Center of Excellence in Topological Quantum Computation and School of Physical Sciences,
University of Chinese Academy of Sciences, Beijing 100190, China*

Barlowite $\text{Cu}_4(\text{OH})_6\text{FBr}$ shows three dimensional (3D) long-range antiferromagnetism, which is fully suppressed in $\text{Cu}_3\text{Zn}(\text{OH})_6\text{FBr}$ with a kagome quantum spin liquid ground state. Here we report systematic studies on the evolution of magnetism in the $\text{Cu}_{4-x}\text{Zn}_x(\text{OH})_6\text{FBr}$ system, as a function of x , to bridge the two limits of $\text{Cu}_4(\text{OH})_6\text{FBr}$ ($x = 0$) and $\text{Cu}_3\text{Zn}(\text{OH})_6\text{FBr}$ ($x = 1$). Neutron diffraction measurements reveal a hexagonal-to-orthorhombic structural change with decreasing temperature in the $x = 0$ sample. While confirming the 3D antiferromagnetic nature of low-temperature magnetism, the magnetic moments on some Cu^{2+} sites in the kagome planes are found to be vanishingly small, suggesting strong frustration already exist in barlowite. Substitution of interlayer Cu^{2+} with Zn^{2+} , with gradually increasing x , completely suppresses the bulk magnetic order at around $x = 0.4$, but leaves a local, secondary magnetic order up to $x \sim 0.8$ with slight decrease of its transition temperature. The high-temperature magnetic susceptibility and specific heat measurements further suggest that the intrinsic magnetic properties of kagome spin liquid planes may already appear from $x > 0.3$ samples. Our results therefore reveal that the $\text{Cu}_{4-x}\text{Zn}_x(\text{OH})_6\text{FBr}$ may be the long-thought experimental playground for the systematic investigations of the quantum phase transition from a long-range antiferromagnet to a topologically ordered quantum spin liquid.

I. INTRODUCTION

A quantum spin liquid (QSL) can be briefly described as a symmetric state without magnetic order emerging from strong quantum fluctuations in frustrated magnetic systems^{1–3}. The quantum fluctuations are usually enhanced by geometrical frustrations of magnetic ions, which are commonly seen in, e.g., triangle, kagome or pyrochlore lattices. Two-dimensional magnetic kagome lattice has attracted a lot of interests in the search for QSLs⁴. Theoretically, it has been shown that the kagome system may exhibit various ordered state and different QSL ground states^{5–18}, such as chiral and Z_2 QSL. These kagome QSLs are usually very close in energy¹⁹ and also depends sensitively on the particular form of the superexchange couplings, which renders them difficult to be testified experimentally.

Experimental progress in finding kagome QSLs has been substantial. Among many kagome magnets, herbertsmithite $\text{ZnCu}_3(\text{OH})_6\text{Cl}_2$ shows several promising properties of a QSL². First of all, it consists of perfect kagome Cu^{2+} ($s = 1/2$) planes that shows no magnetic order down to at least 20 mK^{20–23}. Inelastic neutron scattering (INS) experiments display broad dispersionless magnetic excitations that are consistent with spinon continuum expected in QSLs²⁴. Later nuclear magnetic

resonance (NMR) and INS experiments suggest that the system may be gapped^{25,26}. Interestingly, previous studies have suggested that herbertsmithite may be close to a quantum critical point (QCP)²⁷. However, it is later found that the low-energy spin excitations (< 1 meV) are dominated by the so-called "impurities" of residual interlayer Cu^{2+} ions due to imperfect substitution of inter-kagome Cu by Zn^{26,28}. Moreover, $\text{Cu}_4(\text{OH})_6\text{Cl}_2$, the base material that leads to herbertsmithite, has at least four polymorphs with different nuclear structures that are all different from herbertsmithite and have different magnetic orders^{29–39}. INS experiments also do not support the presence of a QCP in the $\text{Zn}_x\text{Cu}_{4-x}(\text{OD})_6\text{Cl}_2$ system since the antiferromagnetic (AF) order in the $x = 0$ sample is mixed with valence-bond solid (VBS) state and becomes spin-glass-like with increasing x before the QSL is established in the $x = 1$ sample³⁷.

Recently, a new compound of $\text{Cu}_3\text{Zn}(\text{OH})_6\text{FBr}$ has been synthesized to exhibit properties that are consistent with a Z_2 QSL^{40–42}. This compound is obtained by substituting interlayer Cu^{2+} in barlowite $\text{Cu}_4(\text{OH})_6\text{FBr}$ with nonmagnetic Zn^{2+} . The barlowite has perfect Cu^{2+} kagome planes with an AF transition at about 15 K^{43–45}. Since the barlowite and $\text{Cu}_3\text{Zn}(\text{OH})_6\text{FBr}$ have the same space group for the crystal structures at room temperature, it may provide us a rare opportunity to study the

quantum phase transition from an AF ordered state to a QSL ground state by continuously tuning Zn doping level. Therefore, the $\text{Cu}_{4-x}\text{Zn}_x(\text{OH})_6\text{FBr}$ system may provide the long-thought experimental playground for the investigation of novel quantum phase transitions between symmetry-breaking phases and symmetric topologically ordered phases.

In this paper, we systematically investigate the magnetic properties of the $\text{Cu}_{4-x}\text{Zn}_x(\text{OH})_6\text{FBr}$ system. Our results suggest that Zn can indeed be continuously doped into barlowite and suppress the long-range AF order. However, a hexagonal-to-orthorhombic structural change is observed in barlowite and the low-temperature magnetic structure is directly associated with the orthorhombic structure. According to x-ray diffraction and magnetic susceptibility measurements, we find that the interlayer Cu^{2+} ions result in lattice distortion and a local magnetic order up to $x = 0.82$. However, the specific heat measurements suggest that the bulk 3D antiferromagnetic order should disappear around $x = 0.4$ and the spin dynamics of QSL kagome planes may already start to evolve from $x > 0.3$, which finally leads to a gapped QSL in $\text{Cu}_3\text{Zn}(\text{OH})_6\text{FBr}$. Putting these information together, our comprehensive results suggest that the $\text{Cu}_{4-x}\text{Zn}_x(\text{OH})_6\text{FBr}$ system host rich physics of the interplay of frustration, antiferromagnetic order as well as the topologically ordered QSL.

II. EXPERIMENTS

We sealed powders of $\text{Cu}_2(\text{OH})_2\text{CO}_3$, NH_4F , ZnBr_2 and CuBr_2 in a reaction vessel with water, which was slowly heated to 200 °C and kept for 12 hours before cooling down to room temperature. Powders of $\text{Cu}_{4-x}\text{Zn}_x(\text{OH})_6\text{FBr}$ were obtained by drying the products. The Zn content is determined by the inductively coupled plasma mass spectrometer. It should be noted for the $\text{Cu}_3\text{Zn}(\text{OH})_6\text{FBr}$, the Zn content is determined to be about 0.92. We will use actual Zn doping level throughout the paper, so the $x = 0.92$ sample is equivalent to $\text{Cu}_3\text{Zn}(\text{OH})_6\text{FBr}$ reported previously^{40,42}. To obtain the deuterated samples, the mixture is changed to CuO , ZnF_2 , ZnBr_2 and CuBr_2 , and we use heavy water instead. The content of H is less than 2% according to the NMR measurement. The magnetic susceptibility and heat capacity were measured by the MPMS and PPMS (Quantum Design), respectively. The structures of the $\text{Cu}_{4-x}\text{Zn}_x(\text{OH})_6\text{FBr}$ system were measured by the x-ray diffractometer at room temperature. The magnetic and nuclear structures of $\text{Cu}_4(\text{OD})_6\text{FBr}$ are determined by neutron diffraction experiments performed on the SPODI diffractometer at FRM-II, Germany and the HB-2A diffractometer at HFIR, USA, with wavelength of 1.5483 Å and 2.4103 Å, respectively.

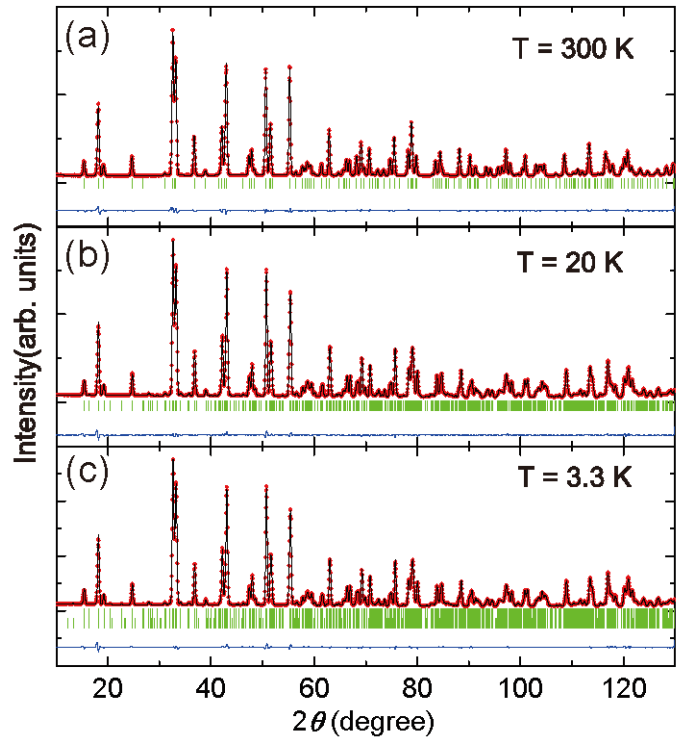


FIG. 1. Neutron powder diffraction intensities of $\text{Cu}_4(\text{OD})_6\text{FBr}$ (red dots) at (a) 300 K, (b) 20 K, and (c) 3.3 K. The calculated intensities are shown by the black lines. Short vertical green lines represents Bragg peak positions. The blue line shows the difference between measured and calculated intensities. The weighted profile R-factor (R_{wp}) is 4.22%, 4.46%, and 4.29% for (a), (b) and (c), respectively.

III. RESULTS

A. Nuclear and magnetic structures in $\text{Cu}_4(\text{OH})_6\text{FBr}$

Figure 1 (a)-(c) show the neutron diffraction and refinement results of $\text{Cu}_4(\text{OH})_6\text{FBr}$ at 300 K, 20 K and 3.3 K, respectively. The refinement of the data at 3.3 K has to include an AF structure as discussed later in this section. The nuclear structure at room temperature is found to be the same as reported previously⁴³. At 20 K, it changes from hexagonal ($P6_3/mmc$) to orthorhombic structure (Pnma) with lattice constants $a_O = 11.5129$ Å, $b_O = 9.2703$ Å and $c_O = 6.6801$ Å. Figure 2(a) depicts the change of the structure in the view vertical to the kagome planes. According to low-temperature structure, we label the three Cu^{2+} ions in the kagome planes as Cu(1), Cu(2a) and Cu(2b), the interlayer Cu^{2+} as Cu(3). At room temperature, the first three of them forms a equilateral triangle. Cu(3) has three equivalent positions with an average position at the center of the triangle, as shown in the left panel of Fig. 2(a). At 20 K, the most significant change is that the Cu(3) picks up

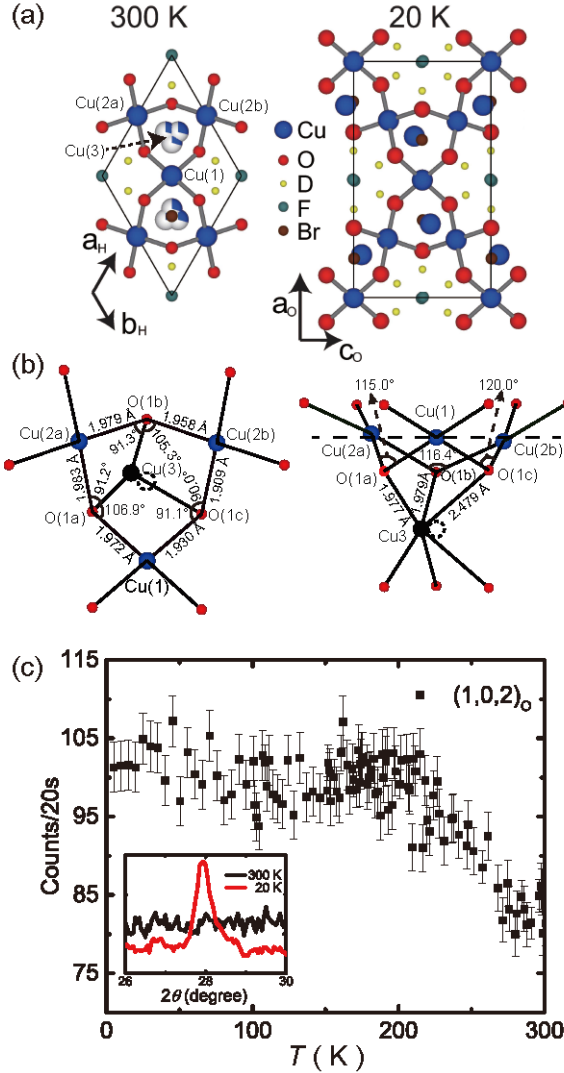


FIG. 2. (a) Nuclear structure at 300 K (left) and 20 K (right) in the view vertical to the kagome plane. The diamond and rectangle are in-plane unit cells at 300 K and 20 K, respectively. The subscripts of "H" and "O" denote hexagonal and orthorhombic structures, respectively. We note that the c-axis at room temperature becomes the b-axis at low temperature. The three overlapping Cu atoms at 300 K represent three positions that the atom may actually occupy. (b) Detailed low-temperature structure showing only Cu (large blue circles) and O (small red circles) in the view parallel to orthorhombic b (left) and orthorhombic a (right), respectively. (c) Temperature dependence of the $(1,0,2)_O$ structural peak. The inset shows 2θ scans around this peak at 20 K and 300 K.

one position and moves closer to Cu(2a) with negligible change of the in-plane distance from 0.3964 to 0.4070 Å. In the meantime, the positions of Cu(2a) and Cu(2b) are distorted both within and out of the kagome plane while that of Cu(1) remains unchanged. The new unit cell is defined according to positions of Cu(1) ions. As a result, the Cu^{2+} kagome planes become significantly distorted.

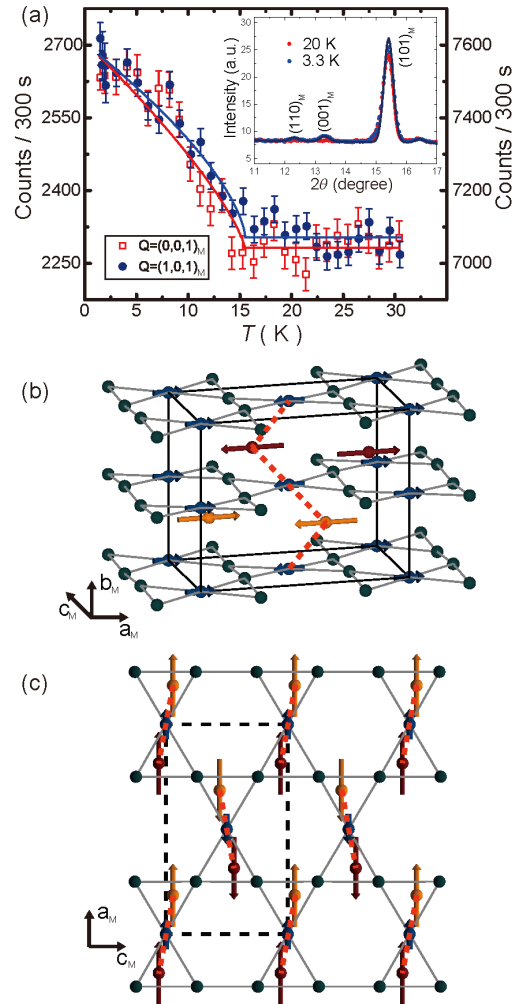


FIG. 3. (a) Temperature dependence of $(0,0,1)_M$ (open red squares) and $(1,0,1)_M$ (filled blue circles) magnetic peaks. The subscript "M" denotes magnetic. The solid lines are the fitted results as described in the main text. The inset shows the refine results of three magnetic peaks. (b) Magnetic structure with the arrows indicating the sizes and directions of magnetic moments on Cu^{2+} ions. The magnetic unit cell is the same as the low-temperature nuclear unit cell as shown by black lines. The red dashed line connects Cu(1) and Cu(3) to forms a ferromagnetic zigzag chain as described in the main text. (c) Magnetic structure viewed vertical to the kagome planes. The red dashed lines are magnetic chains as shown in (b). The solid lines connects the Cu^{2+} ions within the kagome plane. The dashed rectangle represents the magnetic/orthorhombic unit cell.

Figure 2(b) gives the values of the Cu-O bond lengths and Cu-O-Cu angles at 20 K. According to the Goodenough-Kanamori rule^{46,47}, the nearest-neighbour superexchange changes from positive (antiferromagnetic) to negative (ferromagnetic) when the Cu-O-Cu angle goes through about 95° ⁴⁸. The Cu-O-Cu angles between Cu(3) and three other Cu^{2+} have values both larger and smaller than 95° at 20 K, suggesting very complicated

superexchange couplings.

Figure 2(c) shows the temperature dependence of the intensity of the $(1,0,2)_O$ structural peak in the orthorhombic notation, which appears below about 270 K and slowly increases with decreasing temperature until about 200 K. As discussed above, the structural change from high temperature to low temperature is associated with a particular position chosen by Cu(3) from three equivalent positions. Since the position of Cu(3) are randomly distributed among these three positions at room temperature, it follows that Cu(3) ions should be able to resonate among them above 200 K so that their positions are not random any more at low temperature. At current stage, due to the lack of thermodynamic evidence, we are unable to distinguish whether this structural change is a phase transition or rather a crossover resulting from increasing distortion with decreasing temperature.

Assuming that there is no structural transition below 20 K, we find that the neutron diffraction data at 3.3 K (Fig. 1(c)) can be refined by introducing an AF order. To be more explicit, the inset of Fig. 3(a) shows the neutron diffraction data and the refinement results for the first three peaks with lowest angles. Two new peaks emerge at 3.3 K and the intensity of the third peak significantly increases when temperature decreases from 20 K to 3.3 K. The main panel of Figure 3(a) gives the temperature dependence of the intensities of two peaks, which is consistent with the AF transition at about 15 K reported previously⁴³, suggesting their magnetic origin. Within the statistics, only one magnetic transition is observed. With T_N fixed at 15.5 K determined by the specific heat measurements as shown in the next section, the intensities of the $(0,0,1)_M$ and $(1,0,1)_M$ AF Bragg peaks can be fitted by $A(1 - T/T_N)^{2\beta}$ with β as 0.39 ± 0.06 and 0.33 ± 0.04 , respectively. These values of the order parameter critical exponent are consistent with the 3D Heisenberg universality⁴⁹.

Figure 3(b) shows the magnetic structure of $\text{Cu}_4(\text{OD})_6\text{FBr}$ refined from Fig. 1(c), which is an antiferromagnetic order with the propagation vector $k = (0,0,0)$ with a magnetic unit cell same as the orthorhombic one. All magnetic moments point to orthorhombic a direction. Moreover, the sizes of the moments on Cu(1) and Cu(3) are $0.308(3) \mu_B$ and $0.694(2) \mu_B$, respectively, while that on both Cu(2a) and Cu(2b) is just $0.037(2) \mu_B$. Effectively, there is no moments for the distorted Cu^{2+} ions in the kagome planes, which suggests a direct relationship between the magnetic and nuclear structures. Within a kagome plane, the moments of Cu(1) align ferromagnetically along the c_O direction but antiferromagnetically along the a_O direction. To some extend, the magnetic structure here may be treated as a series of ferromagnetic zigzag chains formed by adjacent Cu(1) and Cu(3) within the same plane as indicated by the dashed red line in Fig. 3(b). From the view vertical to the kagome planes, these chains are parallel to each other along the c_M axis and rotates symmetrically along the a_M axis as shown in Fig. 3(c). These weak-linked magnetic chains

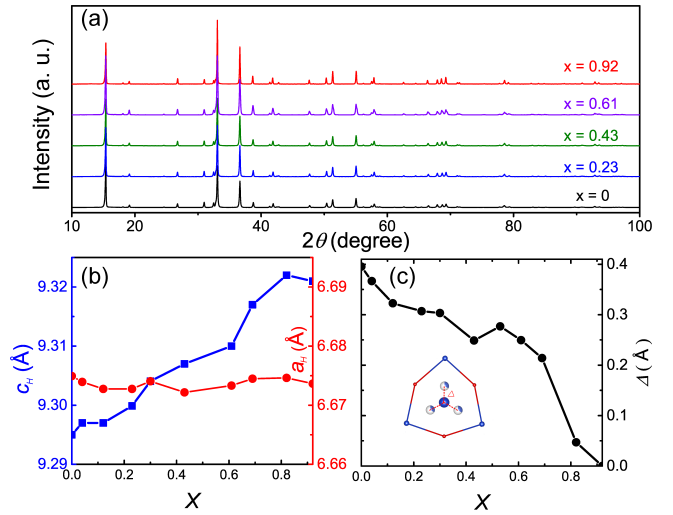


FIG. 4. (a) Room-temperature x-ray diffraction data of selected $\text{Cu}_{4-x}\text{Zn}_x(\text{OH})_6\text{FBr}$ samples. The intensity of each sample has been shifted. (b) Evolution of lattice constants with Zn doping level x at room temperature. We note that $a_H = b_H$. (c) Doping dependence of the splitting Δ of Cu(3) from its average position as defined in the inset.

may explain why T_N can be easily raised by magnetic field⁴³.

B. Evolution of the antiferromagnetic order with Zn doping

Figure 4(a) shows the room-temperature x-ray diffraction data of $\text{Cu}_{4-x}\text{Zn}_x(\text{OH})_6\text{FBr}$ with different x from 0 to 0.92. Since there is no new peak appear with Zn doping, one can conclude that Zn can be continuously doped into barlowite. All the data can be refined by the hexagonal structure with the space group of $P6_3/mmc$. Figure 4(b) gives the doping evolution of lattice constants a_H and c_H . With increasing x , c_H linearly increases while a_H remains the same, which suggests that Zn^{2+} ions only substitute the interlayer Cu^{2+} ions. As discussed in previous subsection, the interlayer Cu^{2+} in barlowite has to be refined with three equivalent positions. One can define Δ as the distance from one of these positions to the center of their average position, as shown by the inset of Fig. 4(c). The value of Δ continuously decreases with increasing x and becomes zero in the $x = 0.92$ sample, as shown in Fig. 4(c). The Cu-O-Cu angle between Zn^{2+} or Cu^{2+} at the Cu(3) position and other Cu^{2+} ions in kagome planes of the $x = 0.92$ sample is 94.73° at 4 K according to our previous measurements⁴², which will give a nearly zero superexchange couplings⁴⁸. Therefore, it seems that the presence of residual interlayer Cu^{2+} will not affect the spin dynamics of the kagome layers as far as its content is less than 10%.

The AF transition in barlowite can be observed in specific heat as reported previously⁴³. Upon Zn doping, the

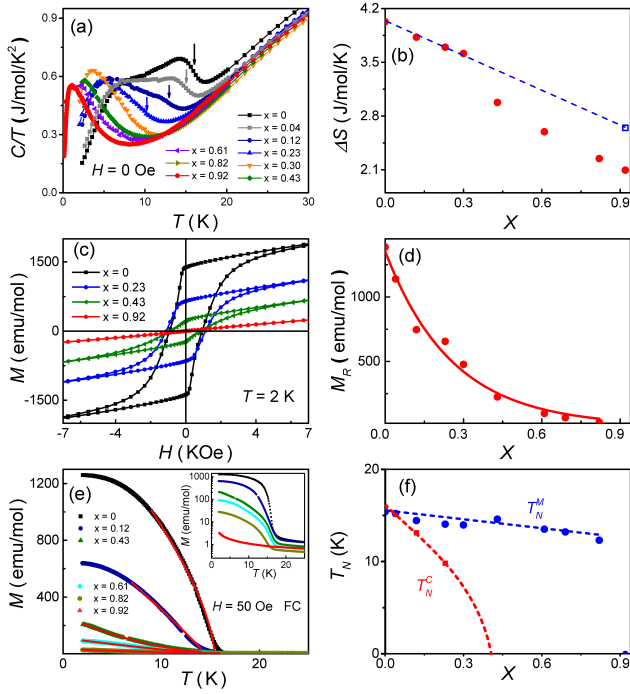


FIG. 5. (a) Low-temperature specific heat of $\text{Cu}_{4-x}\text{Zn}(\text{OH})_6\text{FBr}$. All the samples were measured down to 2 K except for the $x = 0.92$ sample, which has already been reported previously⁴⁰. The arrows indicate the bulk magnetic transition temperature T_N , which is determined as the middle point of the drop of $\Delta C/T$ during the transition. (b) Temperature dependence of ΔS as defined in the main text. The red filled circles are results considering C/T above 2 K while the temperature in obtaining the data of blue open square is down to 50 mK. (c) Field dependence of magnetization at 2 K for selected samples at low fields. (d) Doping dependence of retentivity M_R . The solid line is an exponential fit. (e) Low-temperature magnetic moments of $\text{Cu}_{4-x}\text{Zn}_x(\text{OH})_6\text{FBr}$ measured by field-cooling (FC) process at 50 Oe. The solid lines are fitted results as described in the main text. The inset shows the data with logarithmic scale. (f) Doping dependence of T_N from specific heat (T_N^C , red squares) and susceptibility (T_N^M , blue circles) measurements. The T_N of the $x = 0.92$ sample is manually put as zero. The dashed lines are guides to the eye.

transition can be still seen in the $x = 0.12$ sample, but becomes indistinguishable due to the presence of a large hump at low temperature in C/T for $x \geq 0.3$, as shown in Fig. 5(a). It has been suggested that there is a second magnetic transition just below T_N in barlowite⁴³, but from our data in Fig. 5(a), it is clear that this is due to the low-temperature hump with its temperature increasing with decreasing x . We also note that it has been suggested that this hump, which looks like a plateau in the temperature dependence of C , is due to the contribution from residual interlayer Cu^{2+} in herbertsmithite²⁶, but our results cast shadow upon this statement since the area of the hump seems to change little with doping.

We may estimate the contribution of this hump by analyzing the entropy change ΔS during the magnetic transition. The high-temperature data are fitted by a simple polynomial function $C_{bg} = \alpha T^2 + \beta T^3$ as done previously⁴³. The magnetic part of the specific heat C_M can be obtained by subtracting C_{bg} from the raw data. ΔS can thus be obtained by integrating C_M/T from 0 to 20 K, assuming that $C_M/T(T = 0\text{K}) = 0$, which is the case for either AF ordered or QSL ground state. However, we have only measured the specific heat down to 2 K for most of the samples as shown in Fig. 5(a). The above process will significantly underestimate the contribution below 2 K for samples with large x since the hump temperature becomes smaller than 2 K. We have measured the specific heat of the $x = 0.92$ sample down to 50 mK, which can give us a more precise value of ΔS , as shown by the blue square in Fig. 5(b). A rough linear doping dependence of ΔS from the low-doping samples to $x = 0.92$ sample is found, suggesting that the hump contribution of ΔS is rather independent of doping. Therefore, the actual entropy change of ΔS in barlowite is just about 1.38 J/mol/K, which corresponds to $0.06 k_B \ln 2$ per Cu^{2+} , only about one third of that reported previously⁴³.

Figure 5(c) shows low-temperature field dependence of magnetization M at 2 K. Ferromagnetic-like hysteresis can be found in all the samples except for the $x = 0.92$ one. The doping dependence of retentivity M_R , i.e., the magnetization at zero field after the magnetic field is removed, is shown in Fig. 5(d), where M_R decreases exponentially with increasing x . The presence of ferromagnetic-like hysteresis most likely comes from the domains formed at low temperature due to the orthorhombic structure. The exponential decrease of M_R suggests that either the energy required for overcoming the domain walls or the ferromagnetic-like component of the bulk order decreases quickly with increasing x .

Figure 5(e) shows the temperature dependence of magnetic moment M below 25 K at 50 Oe. The low-temperature signal decreases dramatically with increasing x , but we can still observe magnetic transitions for samples with x up to 0.82. Fitting the data with $A(1-T/T_N)^\beta$ gives the doping dependence of T_N^M in Fig. 5(f), where T_N^M only decreases slightly with increasing x and suddenly becomes zero at $x = 0.92$. On the other hand, T_N^C , obtained from the specific heat measurements in Fig. 5(a), decreases quickly with Zn doping and may become zero around $x = 0.4$.

C. High-temperature and high-field properties of $\text{Cu}_{4-x}\text{Zn}_x(\text{OH})_6\text{FBr}$

Figure 6(a) shows temperature dependence of $1/\chi$ of $\text{Cu}_{4-x}\text{Zn}_x(\text{OH})_6\text{FBr}$. The high-temperature data from 150 K and 300 K can be fitted by the Curie-Weiss function as $\chi = C_{CW}/(T - \theta_{CW})$. The Curie constant C_{CW} decreases linearly with increasing doping, as shown in

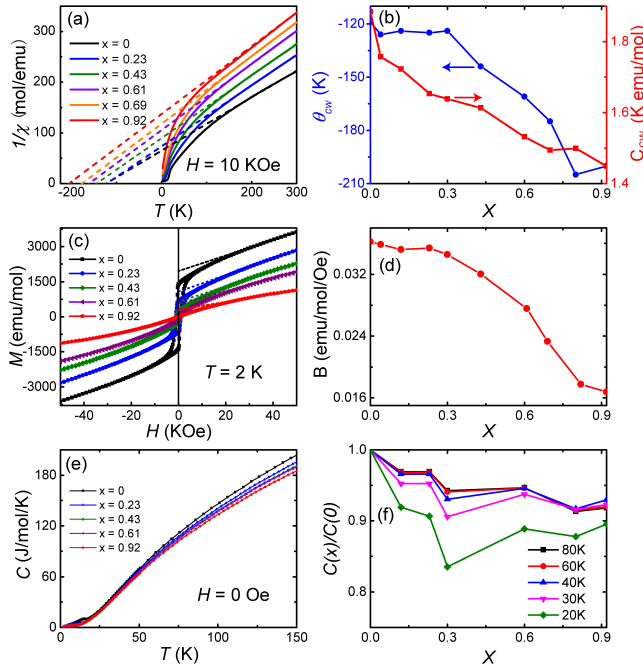


FIG. 6. (a) Temperature dependence of $1/\chi$ for $\text{Cu}_{4-x}\text{Zn}_x(\text{OH})_6\text{FBr}$. The dashed lines are fitted results between 150 K to 300 K. (b) Doping dependence of the Curie temperature θ_{CW} (left axis) and Curie constant C_{CW} (right axis). (c) Field dependence of magnetization at 2 K for selected samples at high fields. The dashed lines are linear fitted results from 30 to 50 K Oe. (d) Doping dependence of the slope B fitted from (c). (e) High-temperature specific heat of selected samples. (f) Doping dependence of $C(x)/C(0)$ at several temperatures.

Fig. 6(b), which suggests that it is associated with the content of Cu^{2+} ions. However, the absolute value of the Curie temperature θ_{CW} only starts increasing above $x = 0.3$, which is consistent with what observed in the $\text{Zn}_x\text{Cu}_{4-x}(\text{OH})_6\text{Cl}_2$ system²⁰. This implies there is a substantial change of the nature of magnetic interactions in the system from $x > 0.3$, and we believe it is related to the appearance of the magnetic properties of the kagome QSL plane from $x > 0.3$ onwards.

Figure 6(c) shows high-field magnetization at 2 K. The data between 30 K Oe to 50 K Oe can be fitted by a linear function as $A + BH$. We note that similar measurements on the single crystal of barlowite have shown large anisotropy for field parallel and perpendicular to c axis, but the slopes in the above field range are rather the same²⁶. Figure 6(d) shows doping dependence of B , which starts decreasing above $x = 0.3$, again signifying the onset of the kagome QSL plane physics.

Figure 6(e) shows the specific heat data up to 150 K. Apart from low-temperature differences due to the presence of the AF order and hump (Fig. 5(e)), the high-temperature data also shows different behaviors. Figure 6(f) plots the doping dependence of $C(x)/C(0)$, where $C(x)$ and $C(0)$ are the specific heat with Zn doping level

of x and zero, respectively. This value roughly decreases monotonically with x for $T > 60$ K, which suggests that the high-temperature specific heat may be dominated by phonons. However, a dip is found at $x = 0.3$ for those at lower temperatures, indicating that there is contribution from kagome QSL plane as suggested in Fig. 6(b) and 6(d). This is also consistent with the observation that only a small amount of entropy is involved during the magnetic transition in barlowite as shown in the previous section.

IV. DISCUSSIONS

Our results provide a comprehensive picture of the magnetic order in barlowite. The establishment of the AF order is directly associated with the structural distortion at high temperature, which is the reason that the magnetic structure in Fig. 3 is different from the incorrectly proposed canted antiferromagnetic order based on the first-principles calculation⁴⁴ without knowing the structural change. It is interesting to note that three different magnetic structures have been proposed for the clinoatacamite $\text{Cu}_4(\text{OH})_6\text{Cl}_2$ ³⁷⁻³⁹. We emphasize that our magnetic structure is consistent with results from bulk measurements on barlowite. For example, the magnetic entropy associated with the magnetic transition is just about $0.06 k_B \ln 2$ per Cu^{2+} . In the simplest model, the magnetic entropy is proportional to M^2 , i.e., the square of magnetic moment⁵⁰. Here the sum of the ordered moments of four Cu^{2+} ions is $1.076 \mu_B$, while the total moment is $4gS = 4.54 \mu_B$, taking $g = 2.27$ and $S = 1/2$ ⁴³. Therefore, the entropy release above the transition is about 5.6% of $k_B \ln 2$, which is very close to the experimental value. Moreover, in the magnetic measurements on the single crystal, the hysteresis loop is only observed when $\mathbf{H} \perp \mathbf{c}$ but not for $\mathbf{H} \parallel \mathbf{c}$ as shown in the single crystal measurements⁴⁵, which is consistent with our results that the magnetic/structural domains only present within the kagome planes. When the magnetic field is parallel to c axis, a saturation moment of $0.29 \mu_B$ per Cu is found⁴⁵. While it is attributed to full polarization of the interlayer Cu^{2+} , we find that this value is close to the sum of the ordered moments in the magnetic chains proposed in our magnetic structure. In $\text{ZnCu}_4(\text{OD})_6\text{Cl}_2$, a VBS state has been found³⁷, although its magnetic structure is still under debates³⁷⁻³⁹. In the case of barlowite, our results suggest that the moments on Cu(2a) and Cu(2b) are effectively zero (Fig. 3(b) and 3(c)), which raises the question whether spins on them may form singlet and leads to other magnetic state such as VBS.

The presence of interlayer Cu^{2+} ions may result in local lattice distortions that will give rise to the magnetic order even when Zn doping level is high. This picture is consistent with our observation of magnetic order in magnetic measurements and low-field hysteresis up to $x = 0.82$, almost doping independence of T_N^M . It also coincides with the nuclear structure refinement results at

room temperature, which suggests that the splitting of Δ of Cu(3) is not zero even when x is as large as 0.82. However, the results from the specific heat measurements provide another picture, where the magnetic order may have already become zero for x larger than 0.4. Since specific heat is a bulk property, it suggests that the magnetic order established at T_N^M is just a secondary phase. This is consistent with our high-temperature and high-magnetic field results, which suggest that the spin dynamics of the QSL kagome plane may indeed start to appear with Zn doping level $x > 0.3$.

Based on these analysis, the magnetic properties in the $\text{Cu}_{4-x}\text{Zn}_x(\text{OH})_6\text{FBr}$ system can be divided into two parts, the one associated with the kagome planes (and thus bulk) and the one associated with interlayer Cu^{2+} moments (and thus local). In very low doping samples, the two parts are strongly coupled and cannot be separated, hence the 3D antiferromagnetic order is formed. With increasing Zn doping, the bulk magnetic order is quickly suppressed and may disappear around $x \sim 0.4$, but the local magnetic order persists up to $x = 0.82$ without much change of its T_N . It is worth noting that in both herbertsmithite and the $x = 0.92$ samples, the spin excitations can be indeed separated into these two independent parts^{26,28,42}.

The suppression of bulk magnetic order gives rise to two possible scenarios. In the first one, a magnetic QCP is present around $x \sim 0.4$, which suggests that $\text{Cu}_{4-x}\text{Zn}_x(\text{OH})_6\text{FBr}$ may provide us the long-thought opportunity to study the quantum phase transition from a magnetic ordered state to a QSL state. On the other hand, it is also possible that the Z_2 QSL state in $\text{Cu}_3\text{Zn}_x(\text{OH})_6\text{FBr}$ is very robust against interlayer magnetic impurities so that it may persists up to very low Zn doping. In this case, the disappearance of the bulk magnetic order may be associated with a first-order quantum phase transition or even phase separation between the 3D AF order and QSL. Either way, the physics is rich and interesting, further studies are needed to clarify the

situation.

V. CONCLUSIONS

Our systematical investigation on the Zn doping effect on the antiferromagnetism in kagome $\text{Cu}_{4-x}\text{Zn}_x(\text{OH})_6\text{FBr}$ system have revealed three major conclusions. First, the magnetic order in barlowite is associated with a hexagonal-to-orthorhombic structural change. Second, Zn doping leads to local lattice distortion and may give rise to phase separation and result in a bulk magnetic order and a local magnetic order. Third, an evolution of spin dynamics in the kagome QSL planes may result in a quantum phase transition around $x = 0.4$ between 3D AF order and QSL. Our results suggest that $\text{Cu}_{4-x}\text{Zn}_x(\text{OH})_6\text{FBr}$ is an interesting system and experimental playground to investigate the intriguing physics of kagome antiferromagnets, and possibly realize the long-thought situation where quantum phase transition between symmetry-breaking and topologically ordered phases. Further works are definitely needed to explore the rich physics in these kagome compounds.

ACKNOWLEDGMENTS

This work is supported by the Ministry of Science and Technology of China (Grants No. 2016YFA0300502, No. 2017YFA0302900, 2016YFA0300604), the National Natural Science Foundation of China (Grants No. 11674406, No. 11374346, No. 11774399, No. 11474330, No. 11421092, No. 11574359 and No. 11674370), the Strategic Priority Research Program(B) of the Chinese Academy of Sciences (XDB07020300, XDB07020000), the key research program of the Chinese Academy of Sciences (XDPB0803) and the National Thousand-Young Talents Program of China. Research conducted at ORNLs High Flux Isotope Reactor was sponsored by the Scientific User Facilities Division, Office of Basic Energy Sciences, US Department of Energy. Z.F. and Y.W. contributed equally to this work.

* ygshi@iphy.ac.cn

† slli@iphy.ac.cn

¹ L. Balents, *Nature* **464**, 199 (2010).

² M. R. Norman, *Rev. Mod. Phys.* **88**, 041002 (2016).

³ L. Savary and L. Balents, *Rep. Prog. Phys.* **80**, 016502 (2017).

⁴ P. A. Lee, *Science* **321**, 1306 (2008).

⁵ S. Sachdev, *Phys. Rev. B* **45**, 12377 (1992).

⁶ H. C. Jiang, Z. Y. Weng, and D. N. Sheng, *Phys. Rev. Lett.* **101**, 117203 (2008).

⁷ S. Yan, D. A. Huse, and S. R. White, *Science* **332**, 1173 (2011).

⁸ H.-C. Jiang, Z. Wang, and L. Balents, *Nat. Phys.* **8**, 902 (2012).

⁹ L. Messio, B. Bernu, and C. Lhuillier, *Phys. Rev. Lett.* **108**, 207204 (2012).

¹⁰ M. Punk, D. Chowdhury, and S. Sachdev, *Nat. Phys.* **10**, 289 (2014).

¹¹ S. Bieri, L. Messio, B. Bernu, and C. Lhuillier, *Phys. Rev. B* **92**, 060407 (2015).

¹² Y. Iqbal, H. O. Jeschke, J. Reuther, R. Valentí, I. I. Mazin, M. Greiter, and R. Thomale, *Phys. Rev. B* **92**, 220404 (2015).

¹³ K. Kumar, K. Sun, and E. Fradkin, *Phys. Rev. B* **92**, 094433 (2015).

¹⁴ S.-S. Gong, W. Zhu, K. Yang, O. A. Starykh, D. N. Sheng, and L. Balents, Phys. Rev. B **94**, 035154 (2016).

¹⁵ H. J. Liao, Z. Y. Xie, J. Chen, Z. Y. Liu, H. D. Xie, R. Z. Huang, B. Normand, and T. Xiang, Phys. Rev. Lett. **118**, 137202 (2017).

¹⁶ J.-W. Mei, J.-Y. Chen, H. He, and X.-G. Wen, Phys. Rev. B **95**, 235107 (2017).

¹⁷ Y.-C. Wang, C. Fang, M. Cheng, Y. Qi, and Z. Y. Meng, ArXiv e-prints (2017), arXiv:1701.01552 [cond-mat.str-el].

¹⁸ Y.-C. Wang, X.-F. Zhang, F. Pollmann, M. Cheng, and Z. Y. Meng, ArXiv e-prints (2017), arXiv:1711.03679 [cond-mat.str-el].

¹⁹ P. Mendels and F. Bert, C.R. Phys. **17**, 455 (2016).

²⁰ M. P. Shores, E. A. Nytko, B. M. Bartlett, and D. G. Nocera, J. Am. Chem. Soc. **127**, 1346213463 (2005).

²¹ F. Bert, S. Nakamae, F. Ladieu, D. L'Hôte, P. Bonville, F. Duc, J.-C. Trombe, and P. Mendels, Phys. Rev. B **76**, 132411 (2007).

²² P. Mendels, F. Bert, M. A. de Vries, A. Olariu, A. Harrison, F. Duc, J. C. Trombe, J. S. Lord, A. Amato, and C. Baines, Phys. Rev. Lett. **98**, 077204 (2007).

²³ J. S. Helton, K. Matan, M. P. Shores, E. A. Nytko, B. M. Bartlett, Y. Yoshida, Y. Takano, A. Suslov, Y. Qiu, J.-H. Chung, D. G. Nocera, and Y. S. Lee, Phys. Rev. Lett. **98**, 107204 (2007).

²⁴ T. H. Han, J. S. Helton, S. Chu, D. G. Nocera, J. A. Rodriguez-Rivera, C. Broholm, and Y. S. Lee, Nature **492**, 406 (2012).

²⁵ M. Fu, T. Imai, T.-H. Han, and Y. S. Lee, Science **350**, 655 (2015).

²⁶ T.-H. Han, M. R. Norman, J.-J. Wen, J. A. Rodriguez-Rivera, J. S. Helton, C. Broholm, and Y. S. Lee, Phys. Rev. B **94**, 060409(R) (2016).

²⁷ J. S. Helton, K. Matan, M. P. Shores, E. A. Nytko, B. M. Bartlett, Y. Qiu, D. G. Nocera, and Y. S. Lee, Phys. Rev. Lett. **104**, 147201 (2010).

²⁸ G. J. Nilsen, M. A. de Vries, J. R. Stewart, A. Harrison, and H. M. Rønnow, J. Phys. Condens. Matter **25**, 106001 (2013).

²⁹ F. C. Hawthorne, Mineral Mg. **49**, 87 (1985).

³⁰ J. B. Parise and B. G. Hyde, Acta Crystallogr. Sect. C **42**, 1277 (1986).

³¹ J. D. Grice, J. T. Szymanski, and J. L. Jambor, Can. Mineral. **34**, 73 (1996).

³² J. L. Jambor, J. E. Dutrizac, A. C. Roberts, J. D. Grice, and J. T. Szymanski, Can. Mineral. **34**, 61 (1996).

³³ T. Malcherek and J. Schlüter, Acta Crystallogr. Sect. B **65**, 334 (2009).

³⁴ X. G. Zheng, T. Mori, K. Nishiyama, W. Higemoto, H. Yamada, K. Nishikubo, and C. N. Xu, Phys. Rev. B **71**, 174404 (2005).

³⁵ X. G. Zheng, T. Kawae, Y. Kashitani, C. S. Li, N. Tateiwa, K. Takeda, H. Yamada, C. N. Xu, and Y. Ren, Phys. Rev. B **71**, 052409 (2005).

³⁶ X. G. Zheng, H. Kubozono, K. Nishiyama, W. Higemoto, T. Kawae, A. Koda, and C. N. Xu, Phys. Rev. Lett. **95**, 057201 (2005).

³⁷ S.-H. Lee, H. Kikuchi, Y. Qiu, B. Lake, Q. Huang, K. Habicht, and K. Kiefer, Nat. Mater. **6**, 853 (2007).

³⁸ J.-H. Kim, S. Ji, S.-H. Lee, B. Lake, T. Yildirim, H. Nojiri, H. Kikuchi, K. Habicht, Y. Qiu, and K. Kiefer, Phys. Rev. Lett. **101**, 107201 (2008).

³⁹ A. S. Wills and J.-Y. Henry, J. Phys. Condens. Matter **20**, 472206 (2008).

⁴⁰ Z. Feng, Z. Li, X. Meng, W. Yi, Y. Wei, J. Zhang, Y.-C. Wang, W. Jiang, Z. Liu, S. Li, F. Liu, J. Luo, S. Li, G. qing Zheng, Z. Y. Meng, J.-W. Mei, and Y. Shi, Chinese Physics Letters **34**, 077502 (2017).

⁴¹ X.-G. Wen, Chinese Physics Letters **34**, 90101 (2017).

⁴² Y. Wei, Z. Feng, W. Lohstroh, C. dela Cruz, W. Yi, Z. F. Ding, J. Zhang, C. Tan, L. Shu, Y.-C. Wang, J. Luo, J.-W. Mei, Z. Y. Meng, Y. Shi, and S. Li, arXiv:1710.02991.

⁴³ T.-H. Han, J. Singleton, and J. A. Schlüter, Phys. Rev. Lett. **113**, 227203 (2014).

⁴⁴ H. O. Jeschke, F. Salvat-Pujol, E. Gati, N. H. Hoang, B. Wolf, M. Lang, J. A. Schlüter, and R. Valentí, Phys. Rev. B **92**, 094417 (2015).

⁴⁵ T.-H. Han, E. D. Isaacs, J. A. Schlüter, and J. Singleton, Phys. Rev. B **93**, 214416 (2016).

⁴⁶ J. B. Goodenough, Journal of Physics and Chemistry of Solids **6**, 287 (1958).

⁴⁷ J. Kanamori, Journal of Physics and Chemistry of Solids **10**, 87 (1959).

⁴⁸ Y. Mizuno, T. Tohyama, S. Maekawa, T. Osafune, N. Motoyama, H. Eisaki, and S. Uchida, Phys. Rev. B **57**, 5326 (1998).

⁴⁹ M. Campostrini, M. Hasenbusch, A. Pelissetto, P. Rossi, and E. Vicari, Phys. Rev. B **65**, 144520 (2002).

⁵⁰ F. Schwabl, *Statistical Mechanics*, 2nd ed., Advanced Texts in Physics (Springer-Verlag Berlin Heidelberg, 2006).